Accepted Manuscript

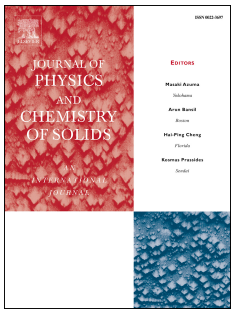

Polyvinylidene fluoride/magnetite nanocomposites: Dielectric and thermal response

C. Tsonos, H. Zois, A. Kanapitsas, N. Soin, E. Siores, G.D. Peppas, E.C. Pyrgioti, A. Sanida, S.G. Stavropoulos, G.C. Psarras

PII: S0022-3697(18)32823-3

DOI: https://doi.org/10.1016/j.jpcs.2019.01.025

Reference: PCS 8887

To appear in: *Journal of Physics and Chemistry of Solids*

Received Date: 15 October 2018

Revised Date: 16 January 2019

Accepted Date: 21 January 2019

Please cite this article as: C. Tsonos, H. Zois, A. Kanapitsas, N. Soin, E. Siores, G.D. Peppas, E.C. Pyrgioti, A. Sanida, S.G. Stavropoulos, G.C. Psarras, Polyvinylidene fluoride/magnetite nanocomposites: Dielectric and thermal response, *Journal of Physics and Chemistry of Solids* (2019), doi: https://doi.org/10.1016/j.jpcs.2019.01.025.

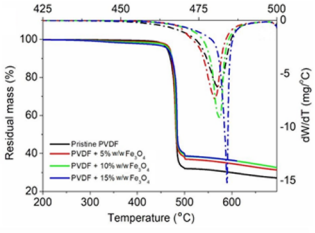

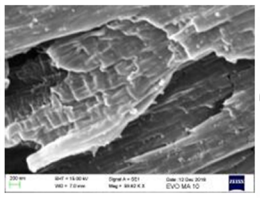

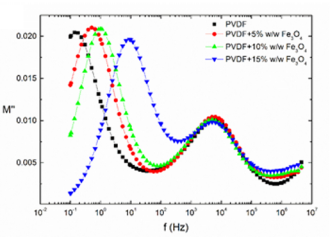

Polyvinylidene Fluoride/Magnetite Nanocomposites: Dielectric and Thermal Response

C. Tsonos[1], H. Zois[2], A. Kanapitsas[1], N. Soin[3], E. Siores[3], G. D. Peppas[4], E. C. Pyrgioti[4], A. Sanida[5], S. G. Stavropoulos[5], G. C. Psarras[5*]

[1] Electronics Engineering Department, Technological Education Institute (TEI) of Sterea Ellada, 35100 Lamia, Greece

[2] Merchant Marine Academy of Epirus, Vathi, 48100 Preveza, Greece

[3] Institute for Materials Research and Innovation (IMRI), University of Bolton, Deane Road, BL3 5AB Bolton, UK

[4] High Voltage Laboratory, Department of Electrical and Computer Engineering, University of Patras, 26504 Patras, Greece

[5] Smart Materials & Nanodielectrics Laboratory, Department of Materials Science, School of Natural Sciences, University of Patras, Patras 26504, Greece

*to whom correspondence should be addressed

Tel.: +30 2610 969347, Fax: +30 2610 969372

E-mail: G.C.Psarras@upatras.gr

Abstract

Nanocomposites of poly (vinylidene fluoride), PVDF, and magnetite (Fe_3O_4) nanoparticles were prepared using the twin screw compounding method and the effect of filler concentration (5-15 wt%) on the thermal stability, dielectric properties and dielectric strength were investigated. It was observed that the dynamic characteristics of crystalline α_c- relaxation peak remain almost constant for the composites studied; while the activation energy plots almost coincide indicating that the time scale of this relaxation process is independent of the Fe_3O_4 filler loading. Ferrite particles alter MWS mechanism behaviour. In the isochronal diagrams of electric modulus dielectric function, at the lower ferrite concentration 5 wt% and the lowest frequency 0.1 Hz, two contributions to MWS process were clearly detected. For ferrite concentrations higher than 5 wt%, seems that the contribution of amorphous-crystalline interfaces to the MWS relaxation drastically decreases and their effect is the broadening of MWS peak at higher temperatures, while the effect of Fe_3O_4-PVDF matrix interfaces dominate in the formation of MWS relaxation. Herein, the nanocomposites dielectric strength performance was investigated by means of switching impulse high voltage stressing and AC (50Hz) high voltage; from the results the nanocomposite demonstrated high levels of dielectrics strength accompanied with stability of performance.

Keywords: A. polymers, A. interfaces, C. differential scanning calorimetry (DSC), C. thermogravimetric analysis (TGA), D. dielectric properties.

Declarations of interest: none

1. Introduction

Magnetic nanoparticle/polymer nanocomposites have recently become one of the most active research areas in the field of materials science and engineering. The electronic, magnetic and optical of these magnetoelectric nanocomposites can be exploited in emerging technological applications in various electronic devices [1–11]. Among the nanosized magnetic fillers for these magnetoelectric composites, magnetite (Fe_3O_4) is of significant interest owing to its strong magnetic response, biocompatiability and low-cost, leading to diverse applications in electronic, magnetic, optical, and mechanical devices [12]. For the polymer matrix, polyvinylidene fluoride (PVDF) is a suitable semi-crystalline polymer owing to its remarkable thermal stability, good chemical resistance and extraordinary pyroelectric and piezoelectric properties [13]. These properties combined with its high elasticity, relative transparency and easy of processing, make this thermoplastic polymer suitable for various technological applications. PVDF shows a complex structure including five distinct crystalline phases related to different chain conformations designed, known as $\alpha, \beta, \gamma, \delta$ and ε phases [14,15]. Amongst them, in terms of its piezoelectric response, β phase is the most active one and, to a lesser extent, the γ phase. Adding nanoparticles to a matrix such as PVDF can enhance its conductive performance and provide advanced response by capitalizing the nature and properties of the nanoscale filler. The final properties of these nanocomposites depend, also, on parameters such as filler size and content, method of preparation and the dispersion of nanoparticles into the polymer matrix [16–20].

Thus, the use of PVDF as matrix in nanocomposites is one of the key parameters for a wide range of applications. Besides the various crystalline phases, the dielectric

response of PVDF is one of the key parameters for applications. Pristine PVDF, depending on its polymorph, shows a dielectric constant close to 10 at room temperature and two main relaxation processes (α_α and α_c). The first one, recorded around 1 MHz, is associated with the cooperative segmental motions within the main chain of the amorphous region during the glass transition (T_g) of the polymer, while the second and slower one is associated with the molecular motions within the crystalline fraction of the polymer [21,22] or/and in the crystal-amorphous interphase region [23]. Moreover, interfacial polarization process plays an important role in neat PVDF, in the cases of high dielectric constant applications. Interfacial polarization is almost always present in polymer based materials due to the existence of heterogeneities. The discontinuity of the dielectric properties implies a trapping of charged ionic/polar species in the interfacial regions of the nanocomposite and consequently a polarization phenomenon can take place. In composite films of PVDF/Fe_3O_4 fabricated through solvent casting method, it was found that the inclusion of nano Fe_3O_4 significantly enhances the crystallinity of PVDF and the β phase contribution [24]. Increased crystallinity enhances, also, the ferrimagnetic properties of these composites whereas the latter improves the thermal stability and polarization effects. Three-phase, carbon nanotubes or graphene nanoplateletes/Fe_3O_4/PVDF nanocomposites have shown a very promising electrical response, which can be exploited in various potential applications in the fields of electromagnetic shielding [25] and energy storage capacitors [26].

However, little work has been done in relation to the influence of Fe_3O_4 nanoparticles on the dielectric response of PVDF nanocomposites [27]. The better and more thorough investigation of dielectric behavior can lead to adequate design with

desirable properties of materials based on PVDF and Fe_3O_4 nanoparticles. In this paper, PVDF-based nanocomposites with varying concentrations of Fe_3O_4 are investigated. The effect of the filler concentration on the thermal response, dielectric properties and dielectric strength are discussed, since they constitute the base of the various potential applications of these materials.

2. Materials and methods

2.1 Materials

Samples composed of PVDF and Fe_3O_4 nanoparticles with a filler content of 0, 5, 10 and 15 wt.% of Fe_3O_4, were prepared using a lab scale twin screw compounder (Thermo Scientific) with counter running screws. A PVDF homopolymer SOLEF 1008 (from Solvay Solexis) with a melt flow index of 8 g/10 min at 230 ^oC (under a load of 2.16 kg) was used as the base polymer. Fe_3O_4 nanoparticle powder was obtained from Sigma-Aldrich with an average particle size of <50 nm and purity >98% according to the supplier's data sheet. For the compounding process, PVDF pellets (500 g) were mixed with the suitable weight of Fe_3O_4 additive and then passed through the twin screw extruder. The extruder temperature profile was set at 150 ^oC (at hopper end) with 10 ^oC incremental changes across the heated barrel with a final temperature of 195 ^oC at the die head. The PVDF-Fe_3O_4 mixture was fed to the counter rotating screw at ~15 rpm feed rate and was moved across the length of the screw at 40% torque corresponding to 350 rpm screw speed. Monofilament from the die head was then passed through a cooling bath using a set of rollers. Consequently, it was passed onto a chopping unit which made homogeneous pellets (~3 mm length) from the monofilament. The pellets were then dried overnight at 75 ^oC to remove the

adsorbed water before further processing. The twin screw compounding enables higher quality of mixing at lower melt temperatures, thereby avoiding the material degradation at higher temperatures. To obtain the PVDF-Fe_3O_4 thick film samples, hot-press technique was utilized wherein ~55 g of the compounded sample was pressed in between two flat Al plates at a pressure of 40kg/cm^2 for a duration of 2 min 30 sec and then allowed to cool down under the same applied pressure using a cold press. The final sample weight of the PVDF-Fe_3O_4 thick film samples was ~48 g, with the rest of additive mix lost due to the polymer overflow to the outside of the mould. The obtained samples were then used as it is without any further processing.

2.2 Experimental Methods

The surface morphology of the samples was examined using scanning electron microscopy (SEM) by employing an EVO MA-10 Carl Zeiss system. Thermal response and degradation of the PVDF-Fe_3O_4 systems were studied *via* Thermogravimetric Analysis (TGA) using a TA Q500 instrument (TA Instruments), in the temperature range 30-700^oC, for which the samples were placed in a platinum boat and scans run at 10^oC/min under dry Nitrogen atmosphere, while the thermal transitions of the samples were investigated by Differential Scanning Calorimetry (DSC) using a DSC Q200 (TA instruments).

The dielectric response of the pristine PVDF matrix and PVDF-Fe_3O_4 nanocomposites was assessed by means of Dielectric Relaxation Spectroscopy (DRS). The experimental setup for dielectric measurements includes an Alpha-N Frequency Response Analyzer, Novotherm system for temperature control, BDS1200 dielectric

cell with two gold plated parallel electrodes, and Windata software for controlling the whole experimental setup and data acquisition. All devices were supplied by Novocontrol Technologies. The frequency range of the applied field was varying from 10^{-1} Hz to 10^{7} Hz, in the temperature range of 30-120 ^{o}C. Data were recorded under isothermal frequency scans with a temperature step of 5^{o}C. The amplitude of the frequency dependent voltage was 1V for all the recorded spectra.

The dielectric strength of the nanocomposites was studied by means of a high voltage test transformer (HIGH VOLT GmbH Transformer PEOI 40/100 100kV), controlled by a Siemens Control panel. A two stage Marx impulse generator (Haefely Ltd. 400kV – 1.2kJ) was used to investigate the impulse voltage performance of the nanocomposites. A custom-made test cell made of Plexiglas^{TM} filled with natural ester oil, having a capacity of 1400ml was connected to the AC high voltage transformer through Rogowski electrode configuration. In order to avoid the flashover as well as maintain the homogenous electric field, the nanocomposites of dimensions 150 mm x 90 mm x 1 mm were connected to the Rogowski electrodes and then placed into the natural ester dielectric liquid for measurements.

3. Results and discussion

3.1 Thermal properties

Fig. 1 shows representative cryo-fractured SEM images of the PVDF-Fe_3O_4 nanocomposites containing 5 and 15 wt% Fe_3O_4 nanoparticles. The presence of Fe_3O_4 particles shows a good distribution across the PVDF matrix without significant agglomeration. Furthermore, on increasing the Fe_3O_4 particle concentration to 15

wt%, larger agglomerates of Fe_3O_4 were observed with mean diameter in the range ~200 nm.

It is well established that the thermal properties of the nanocomposites are affected by the presence of filler particles which lead to the formation of an interfacial layer between the nanoparticles and the polymer matrix while affecting the crosslinking procedure. The effect of Fe_3O_4 nanoparticles on thermal stability of the PVDF matrix was studied using thermogravimetric analysis. Typical traces of TGA thermograms for the pristine PVDF matrix and the PVDF-Fe_3O_4 composite systems are shown in Fig. 2a. The results reveal that all the samples show good thermal stability for temperatures up to around 450 ^oC with a maximum decomposition temperature higher than 470 ^oC (~480 ^oC) with a significant weight loss occurring between 450-510 ^oC, corresponding to the decomposition of the PVDF matrix. This decomposition temperature is the temperature corresponding to the inflection point of the thermal degradation curves and is considered as the temperature of the peak of the derivative mass loss (DTGA) curve, i.e. the temperature of the maximum reaction (weight loss) rate, as shown in Fig. 2a. It can be observed that the nanocomposites display enhanced thermal properties. At lower filler loadings (5 wt%), while the degradation temperature is marginally lowered, for 10 wt% and 15 wt% composites, not only the degradation temperatures became marginally higher (~484 ^oC for 15wt% composite vs. ~481 ^oC for pristine PVDF), but the degradation peak also becomes narrower. The temperature corresponding to 5 % initial mass loss, $T_{5\%}$, (onset of the TGA curve) is indicative of the thermal stability of the samples. The variation of $T_{5\%}$ with filler content is shown in Fig. 2b-left axis, wherein the data reveal that the pristine matrix shows, generally, lower weight loss onset (i.e. the degradation starts at lower

temperatures), as compared to the nanocomposites. In the case of nanocomposites, the $T_{5\%}$ temperature is slightly reduced with the increase of the Fe_3O_4 nanoparticles' content. From the variation of the mass loss rate (dW/dT) curve as a function of the filler content, it can be observed that the presence of Fe_3O_4 nanoparticles enhances the mass loss rate. The increasing trend observed for the samples with higher filler concentration can be attributed to the fact that the degradation process of the nanocomposites is enhanced by the Fe_3O_4 nanoparticles [28].

DSC measurements reveal a double melting peak in all samples (Fig. 3a) during the first heating scan. A main peak around 175 °C and a shoulder around 168 °C were observed for the pure PVDF. Generally, the existence of double melting peak is attributed to the presence of crystallites of different thickness, variety of crystallites perfection, re-melting of crystallites formed during heating or existence of polymorphism [24]. During the first cooling scan from melt (Fig. 3b), a single crystallization peak was found and the crystallization temperature, T_c, of pure PVDF was observed at 138 °C, while for nanocomposites, a narrower crystallization peak and a shift of crystallization temperature T_c to higher temperatures (3-5 °C) compared to pure PVDF was detected. The increase of T_c upon addition of Fe_3O_4 is a clear indication of their essence as nucleating agents promoting heterogeneous crystallization, a feature commonly observed in polymer nanocomposites [29,30], while narrowing of the crystallization peak implies a narrower crystallite size distribution [31]. Crystallization (T_c) and melting (T_m) temperatures together with the degree of crystallinity X_c of each sample are presented in Table I. The degree of crystallinity slightly increases by the addition of Fe_3O_4 even for the lowest concentration. For the higher Fe_3O_4 content, a decrease of the degree of crystallinity

was observed. The reduction in the crystallinity, at highest Fe_3O_4 content, can be attributed to the inhibition effect of Fe_3O_4 addition on polymer crystal formation, similar to what has been observed with various other inorganic fillers. A similar reduction in the crystallinity has been observed [32,33].

3.2 Dielectric response

The recorded dielectric spectroscopy data was obtained in terms of complex dielectric permittivity (ε*) which can be separated into its capacitive and conductive components, thus giving the real part of permittivity (ε') and loss factor (ε''). The complex permittivity itself is defined by the following equation:

$$\varepsilon^*(\omega) = \varepsilon'(\omega) - i \cdot \varepsilon''(\omega) \quad (1)$$

where ε' is the real part of permittivity, ε'' is the imaginary part of permittivity and $\omega = 2\pi f$ is the angular frequency of the applied electric field. Fig. 4(a) represents the frequency dependence of ε' for the pristine PVDF as well as the PVDF/Fe_3O_4 nanocomposites (at a fixed temperature of 30 ^oC). It can be clearly observed that the dielectric permittivity is dependent on both frequency and filler fraction loading. As expected, the dielectric constant for PVDF/Fe_3O_4 nanocomposites increases with the increase in the Fe_3O_4 filler content, with the pristine PVDF showing a value of 12 (at 10 Hz) to a maximum value of 15.8 (at 10 Hz) for the 15wt% Fe_3O_4 nanocomposite [34,35]. The ‘‘step- like’’ increase in the ε' values observed at ~ 1 MHz, is related to micro-scale motions of the polymer chain and can be attributed to the glass transition mechanism of PVDF matrix [36] and is denoted as α_α-relaxation. For temperatures

close to the glass transition temperature, segmental mobility is facilitated as large parts of macromolecular chains obtain sufficient thermal energy and dipoles are able to follow the alternating field leading to an increase in permittivity values. On the other hand, the sharp increase in the low-frequency region (below 1 Hz) is identified as the crystalline chain relaxation in PVDF, namely α_c-process. It is associated with the molecular motions in PVDF crystalline region. The origin of this process is attributed to isolated amorphous portions restricted in the crystalline phase [37] or to imperfections and defects in the crystalline structure like, discontinuities, chain loops at the surface of lamella, and chain twisting [38]. Moreover, Fe_3O_4 filled samples show higher values of dielectric permittivity compared to the pristine PVDF matrix, as a result of the incorporation of Fe_3O_4 particles [34,35]. Similar results have been observed in many composites based on PVDF and can be attributed to the increment in the dipolar contribution [39,40].

Now, the real and imaginary parts, ε' and ε'' of the complex dielectric function can be used to calculate the dielectric loss tangent which is defined by the following relationship:

$$\tan\delta = \frac{\varepsilon''}{\varepsilon'} \tag{2}$$

Fig. 4(b) shows the isothermal plots of the dielectric loss tangent tan δ as a function of frequency, at a fixed temperature 30 ^{o}C, for both the PVDF matrix and nanocomposite samples. For all the samples, the tan δ takes a value of less than 0.1 across the frequency spectrum. At the temperature of 30 ^{o}C, two relaxation processes are

evident. The faster segmental relaxation shown at frequency ~4 MHz (although not well-configured due to limitations of our experimental "window" and instrumental constraints) is attributed to the glass-rubber transition relaxation and is denoted as α_α-relaxation. It is well reported that this high-frequency peak is related to the micro-Brownian cooperative motions of the main chain backbone and is considered as the dielectric manifestation of the glass transition temperature of PVDF [41].

The presence of Fe_3O_4 particles, affects only slightly the segmental process (glass-rubber transition relaxation, α_a-process), confirming that the relaxation time and length scale of the α_a-process are practically unaffected by the filler particles. Similar observations have been reported for other polymer composites [42,43]. Also note that the magnitude of the α_α-mechanism remains almost constant which implies that the addition of Fe_3O_4 particles has no significant influence on the amorphous PVDF regions, which contribute to α_α-relaxation, and does not apply restrictions to the re-arrangement of amorphous chains. The slower relaxation peak at about 3 Hz denoted as α_c-relaxation is associated with the molecular motions in the crystalline region of PVDF [44]. While the magnitude of α_c-relaxation increases slightly by the addition of Fe_3O_4 particles, the frequency peak of this mechanism is almost unaffected by the addition of the filler. Similar effect has been observed in many PVDF-filled composites and nanocomposites [27]. It has been reported in the literature [24,32] that, the incorporation of nano-sized ferrite particles in the PVDF matrix, reduces crystalline α-phase of PVDF. Added Fe_3O_4 particles interact with the PVDF matrix, since they play the role of nuclei for PVDF crystallization. So, the kinetics of

crystallization alters in such a way that polar β-phase predominates over non-polar α-phase favors the improvement of ionic mobility and conductivity too [45].

Electric modulus (M*), defined as the inverse quantity of complex permittivity is given by the following relationship:

$$M^*(\omega) = \frac{1}{\varepsilon^*(\omega)} = M'(\omega) + i \cdot M''(\omega) = \frac{\varepsilon'(\omega)}{\varepsilon'(\omega)^2 + \varepsilon''(\omega)^2} + i \cdot \frac{\varepsilon''(\omega)}{\varepsilon'(\omega)^2 + \varepsilon''(\omega)^2} \quad (3)$$

where ε', M' are the real and ε", M" the imaginary parts of dielectric permittivity and electric modulus, respectively. Dielectric permittivity data were transformed via Eq. 3, to the electric modulus formalism. The electric modulus formalism was introduced by McCrum et al. [46] and has been used to study the electrical relaxation phenomena polymers [42,47–49]. This formalism is especially used as it excludes phenomena such as electrode polarization and space charge injection which leads to high values of permittivity and conductivity, especially at high temperatures and low frequencies. Examples and extended arguments of the resulting benefits of electric modulus presentation have been exhibited and discussed elsewhere [47,50].

In Fig. 5(a), the comparative plots of the imaginary part of electric modulus (M") versus frequency, for the pristine PVDF and PVDF/Fe_3O_4 nanocomposites at a constant temperature (T= 100 ^oC) are shown. The recorded peaks clearly show the presence of two relaxation processes. The recorded loss peaks, located in the low and intermediate frequency region, are assigned to Maxwell-Wagner-Sillars (MWS) and crystalline relaxation mechanism, respectively [36]. The relaxation peak at

intermediate frequencies (at about 6 kHz) is identified as the crystalline relaxation (α_c) as discussed earlier. Note that this mechanism has been observed at lower frequency (~3 Hz) at temperature 30 ^{o}C, (see Fig. 3(b)). It is well-known that the dielectric peaks, being thermal activated processes, shift to a higher frequency with increasing temperature. The second peak of the modulus spectra, observed in the low-frequency region (10^{-1}–10 Hz), is attributed to MWS interfacial polarization, which is observed in heterogeneous materials [48,51,52].

In polymers and composites, interfacial polarization is present due to the differences in the permittivity and conductivity values of the filler and polymer matrix. It is well known that the MWS mechanism appears in complex systems exhibiting electrical heterogeneity, due to the accumulation of charges at the interfaces between amorphous and crystalline regions of the polymer or matrix and filler, where they form large dipoles contributing to the achieved polarization [44,53,54].

The shape and magnitude of the crystalline relaxation peak remains almost constant for the studied composites, while it has lower magnitude, compared to the MWS one. In the pristine PVDF matrix, the MWS relaxation occurs due to the interface between amorphous and crystalline regions, whereas in the PVDF/Fe_3O_4 nanocomposites, this low-frequency mechanism strongly depends on the filler content. The increase of Fe_3O_4 concentration shifts this mechanism to higher frequencies i.e. it becomes faster.
In Fig. 5(b), for all the systems studied in this work, the loss modulus index (M") as a function of temperature, measured at a constant frequency of f= 0.1 Hz is presented. This frequency corresponds to a time scale equal to 10 sec, where the DRS has it’s

maximum resolution in the present measurements. As a result, the contributions to MWS relaxation from different interfaces, which slightly vary in their relaxation times, superimpose forming broad peaks. We observe that for the chosen frequency, the loss peak position has a quite a wide variation. The peak temperature decreases with increasing Fe_3O_4 content. It varies from about 100 ^oC (for the pristine PVDF) to almost 50 ^oC (for the sample PVDF+15wt% Fe_3O_4).

A possible explanation for this interesting result could be following: as mentioned earlier, the pristine PVDF matrix shows a MWS type relaxation, which occurs due to the interface between the amorphous and the crystalline regions of the polymeric matrix. This mechanism has a clear, single maximum value at about 100 ^oC. Upon the addition of Fe_3O_4 nanoparticles, two different types of interfaces are formed: an interface between the crystalline regions and amorphous matrix and an interface between the PVDF matrix and the Fe_3O_4 filler particles. Thus, the incorporation of Fe_3O_4 particles generates a second MWS mechanism, due to the creation of additional interfaces between ferrite particles and the PVDF matrix. It is worth mentioning that this second additional mechanism for the sample PVDF+5 wt% Fe_3O_4 lies at a lower temperature as compared to the MWS relaxation of the pristine PVDF matrix, being faster and characterized by shorter relaxation time. For ferrite concentrations higher than 5 wt%, it seems that the contribution of amorphous-crystalline interfaces to the MWS relaxation drastically decreases and its effect is manifested in the broadening of MWS peak at higher temperatures region. At higher ferrite content, the effect of Fe_3O_4-PVDF matrix interface dominates the formation of MWS relaxation. In fact, for the PVDF/Fe_3O_4 nanocomposites, the ferrite particles seem to influence

significantly the MWS mechanism of PVDF matrix, even at the lower filler content. In particular, for the 5wt% Fe_3O_4 sample, these two relaxations overlap each other. The peak observed at about 65 ^oC is attributed to the interfaces between Fe_3O_4 particles and the PVDF matrix, while the shoulder at about 95 ^oC is, unambiguously, ascribed to the interfaces between crystalline regions and amorphous PVDF matrix. The contribution of Fe_3O_4 particles is clearly observed, but the contribution from the polymer matrix is still remarkable, for the 5wt% Fe_3O_4 sample. At increased ferrite concentrations, the second MWS mechanism, owing to the creation of additional interfaces between ferrite particles and the PVDF matrix, dominates and the PVDF peak declines, in fact, besides the increase in the interfaces implies an augmentation of the interfacial polarization phenomena.

In order to further analyze the molecular dynamics of the observed mechanism and to calculate the corresponding activation energies, Arrhenius plots are used as shown in Fig. 6. The temperature dependence of a relaxation process can be analyzed by plotting the frequency of loss maximum versus the reciprocal temperature. The frequency of loss maximum has been obtained from the plots of the imaginary part of electric modulus (M") versus frequency at different temperatures, for all the studied nanocomposites. In Fig. 6(a), the Arrhenius diagram for the local crystalline α_c-relaxation, associated with the molecular motion in PVDF crystalline regions, is presented. Similar plot for MWS process, related to the interfaces between the amorphous and crystalline regions in the pristine PVDF matrix, is shown in Fig. 6(b). The dynamics of the glass transition mechanism were not analyzed as its characteristics are out of the frequency/temperature window of our measurements. It

is well known [38,49,55] that the dynamics of both α_c - mode and MWS mechanism follow linear Arrhenius- type behaviour, given by:

$$f_{max} = f_0 \exp(-\frac{E}{kT}) \quad (4)$$

where f_{max} is the frequency maximum in the imaginary part of modulus spectra, f_0 is the pre-exponential factor, k is the Boltzmann constant (k= 1.381×10^{-23} J/K) and E is the activation energy. The calculated activation energy for the observed relaxation processes can be found in Table II.

Filled samples have higher activation energy values for α_c- mechanism, compared to the pure PVDF matrix. These values are in very good agreement with those found by other researches [56,57] in similar composites. We also observe that the activation energy plots for the crystalline α_c- relaxation almost coincide, which indicates that time scale of this relaxation process is independent of the filler loading. Similar result has been reported for PVDF/$BaTiO_3$ nanocomposites, too [27].

The MWS relaxation for the nanocomposites studied shows also Arrhenius-type behaviour, indicating that this relaxation is a thermally activated process. However, the activation energy of the MWS relaxation is significantly reduced in the nanocomposites as compared to the pristine PVDF matrix. For the nanocomposite samples, the increase in the Fe_3O_4 concentration, leads to increased activation energy values. That is a clear indication that the ferrite particles alter the MWS mechanism behaviour. As the filler concentration increases, the inter-particle distances start to reduce, which could have two different effects. The first one is that it increases the

quantity of polymer chains with restricted mobility around the filler particles which could lead to gradual increase in the activation energy for MWS relaxation [38]. On the other hand, the blocking of charges at the filler-polymer matrix interfaces can described by charging–discharging of a double layer characterized in analogy by a Debye–type length L_D [58]. As the filler concentration increases the distance, L, between the Fe_3O_4 nanoparticles becomes smaller resulting in a lower value of MWS relaxation time because $\tau_{MWS} \propto L_D$ [58]. This effect could explain the shift to higher frequencies of the MWS mechanism with increasing filler concentration, as the content of Fe_3O_4 nanoparticles increases the MWS relaxation becomes faster.

3.3 Dielectric strength measurements

Table III depicts the results of the AC breakdown test measurements for pristine PVDF and PVDF/Fe_3O_4 nanocomposites. Fig. 7 shows a typical representative graph demonstrating the breakdown event recorded during the dielectric strength measurement. The vide ante discharge is accompanied with a current of 18mA, which is decreased while increasing the concentration of the nanoparticles inside the matrix. The breakdown stressed nanocomposites were penetrated after the AC test (Fig. 8). The AC (50Hz) electric field endurance was in the range of 9-22kV/mm.

Based on the same custom cell with the Rogowski electrodes configuration, the nanocomposites were stressed under an impulse voltage of 200/2500μs according to the ASTM D3246-97 standards [59] by means of a two stage Marx impulse voltage generator (Haefely Ltd., 400kV – 1.2kJ). The result of the measurement depicted in

Fig. 9 demonstrates the impulse test, wherein 90μs breakdown occurs at 41kV. It is of great importance that all the studied nanocomposites along with the pristine matrix maintain the same impulse voltage breakdown voltage level of 41kV. This is interpreted as a stability of the overall performance of the aforementioned nanocomposites, despite their nanoparticles' addition or concentration.

The breakdown event as depicted per Fig. 9, is identical for all the nanocomposites regardless of the filler concentration wherein the time to breakdown was constant in the range of 80-95μs, while the maximum impulse voltage withstand level varied between 40-42 kV. In addition, there were no pre-breakdown phenomena, such as corona or early ionization prior to the breakdown of the nanocomposites. The nanocomposites demonstrate a stable dielectric performance and insulating properties *via* the addition of semiconducting nanoparticles, as described from Tanaka [60] which is correlated with the proper preparation and fabrication of the nanocomposites.

4. Conclusions

In conclusions, PVDF/Fe_3O_4 nanocomposites were prepared by twin screw compounder method and characterized. PVDF nanocomposites display enhanced thermal properties. At higher Fe_3O_4 content, the degradation temperatures became marginally higher, while the degradation peak becomes narrower. The degree of crystallinity slightly increases by the addition of Fe_3O_4 even for the lowest concentration, while for the higher Fe_3O_4 content a decrease was observed. Two dielectric relaxations were extensively studied, the α_c-relaxation and MWS interfacial polarization. The dynamic characteristics of crystalline α_c-relaxation remain almost unaffected for the composites, which indicates that time scale of this relaxation

process is independent of the Fe_3O_4 filler loading. The clear contribution of two factors that create the MWS process is rising at lowest Fe_3O_4 concentration and maximum time scale resolution of DRS measurements in the present study. For Fe_3O_4 content higher than 5 wt%, the contribution of amorphous-crystalline interfaces to the MWS relaxation drastically decreases, while the effect of Fe_3O_4-PVDF matrix interfaces dominate in the formation of MWS relaxation. The nanocomposites demonstrated an unprecedented stability of performance during the impulse voltage stressing, wherein a breakdown voltage level of 40-42kV was preserved regardless the nanoparticles concentration; while the nanocomposite maintain high dielectric strength properties under AC voltage (utility frequency).

This work received no funding.

References

[1] Z.-S. Wu, W. Ren, D.-W. Wang, F. Li, B. Liu, H.-M. Cheng, High-Energy MnO_2 Nanowire/Graphene and Graphene Asymmetric Electrochemical Capacitors, ACS Nano. 4 (2010) 5835–5842. doi:10.1021/nn101754k.

[2] B. Weidenfeller, M. Höfer, F. Schilling, Thermal and electrical properties of magnetite filled polymers, Compos. Part A Appl. Sci. Manuf. 33 (2002) 1041–1053. doi:10.1016/S1359-835X(02)00085-4.

[3] A. Sanida, S.G. Stavropoulos, T. Speliotis, G.C. Psarras, Magneto-Dielectric Behaviour of M-Type Hexaferrite/Polymer Nanocomposites., Mater. (Basel, Switzerland). 11 (2018). doi:10.3390/ma11122551.

[4] L.A. Ramajo, A.A. Cristóbal, P.M. Botta, J.M. Porto López, M.M. Reboredo,

M.S. Castro, Dielectric and magnetic response of Fe_3O_4/epoxy composites, Compos. Part A Appl. Sci. Manuf. 40 (2009) 388–393. doi:10.1016/j.compositesa.2008.12.017.

[5] N. Frickel, M. Gottlieb, A.M. Schmidt, Hybrid nanocomposites based on superparamagnetic and ferromagnetic particles: A comparison of their magnetic and dielectric properties, Polymer (Guildf). 52 (2011) 1781–1787. doi:10.1016/J.POLYMER.2011.02.025.

[6] Y. Wang, T. Herricks, M. Ibisate, P.H.C. Camargo, Y. Xia, Synthesis and characterization of monodisperse colloidal spheres of Pb containing superparamagnetic Fe_3O_4 nanoparticles, Chem. Phys. Lett. 436 (2007) 213–217. doi:10.1016/j.cplett.2007.01.046.

[7] G. Zhao, J. Wang, Y. Li, X. Chen, Y. Liu, Enzymes Immobilized on Superparamagnetic Fe_3O_4 @Clays Nanocomposites: Preparation, Characterization, and a New Strategy for the Regeneration of Supports, J. Phys. Chem. C. 115 (2011) 6350–6359. doi:10.1021/jp200156j.

[8] X.W. Dong, K.F. Wang, J.G. Wan, J.S. Zhu, J.M. Liu, Magnetocapacitance of polycrystalline $Bi_5Ti_3FeO_{15}$ prepared by sol-gel method, J. Appl. Phys. 103 (2008) 0–4. doi:10.1063/1.2908219.

[9] Y.W. Bai, W.C. Kuo, Design and implementation of an automatic measurement system for DC-DC converter efficiency on a motherboard, 2010. doi:10.1109/IECON.2010.5675492.

[10] A. Sanida, S.G. Stavropoulos, T. Speliotis, G.C. Psarras, Development, characterization, energy storage and interface dielectric properties in $SrFe_{12}O_{19}$/ epoxy nanocomposites, Polymer (Guildf). 120 (2017) 73–81.

doi:10.1016/j.polymer.2017.05.043.

[11] M. Vadivel, R.R. Babu, K. Ramamurthi, M. Arivanandhan, Enhanced dielectric and magnetic properties of polystyrene added $CoFe_2O_4$ magnetic nanoparticles, J. Phys. Chem. Solids. 102 (2017) 1–11. doi:10.1016/j.jpcs.2016.10.014.

[12] G.A. Prinz, Magnetoelectronics, Science. 282 (1998) 1660–1663. doi:10.1126/science.282.5394.1660.

[13] V. Sencadas, M.V. Moreira, S. Lanceros-Méndez, A.S. Pouzada, R. Gregório Filho, α- to β Transformation on PVDF Films Obtained by Uniaxial Stretch, Mater. Sci. Forum. 514–516 (2006) 872–876. doi:10.4028/www.scientific.net/MSF.514-516.872.

[14] M.G. Broadhurst, G.T. Davis, J.E. McKinney, R.E. Collins, Piezoelectricity and pyroelectricity in polyvinylidene fluoride—A model, J. Appl. Phys. 49 (1978) 4992–4997. doi:10.1063/1.324445.

[15] A.J. Lovinger, Annealing of poly(vinylidene fluoride) and formation of a fifth phase, Macromolecules. 15 (1982) 40–44. doi:10.1021/ma00229a008.

[16] C.K. Chiang, R. Popielarz, Polymer Composites with High Dielectric Constant, Ferroelectrics. 275 (2002) 1–9. doi:10.1080/00150190190021786.

[17] H. Ishida, S. Campbell, J. Blackwell, General Approach to Nanocomposite Preparation, Chem. Mater. 12 (2000) 1260–1267. doi:10.1021/cm990479y.

[18] T.A. Ezquerra, J.C. Canalda, A. Sanz, A. Linares, On the electrical conductivity of PVDF composites with different carbon-based nanoadditives, Colloid Polym. Sci. 292 (2014) 1989–1998. doi:10.1007/s00396-014-3252-6.

[19] R.A. Senthil, J. Theerthagiri, J. Madhavan, S. Ganesan, A.K. Arof, crossmark, J. Phys. Chem. Solids. 101 (2017) 18–24. doi:10.1016/j.jpcs.2016.10.007.

[20] R.A. Senthil, J. Theerthagiri, J. Madhavan, Journal of Physics and Chemistry of Solids Organic dopant added polyvinylidene fluoride based solid polymer electrolytes for dye-sensitized solar cells, 89 (2016) 78–83. doi:10.1016/j.jpcs.2015.11.003.

[21] V. Sencadas, C.M. Costa, V. Moreira, J. Monteiro, S.K. Mendiratta, J.F. Mano, S. Lanceros-Méndez, Poling of β-poly(vinylidene fluoride): dielectric and IR spectroscopy studies, E-Polymers. 5 (2005). doi:10.1515/epoly.2005.5.1.10.

[22] V. Sencadas, S. Lanceros-Méndez, R. Sabater I Serra, A. Andrio Balado, J.L. Gómez Ribelles, Relaxation dynamics of poly(vinylidene fluoride) studied by dynamical mechanical measurements and dielectric spectroscopy, Eur. Phys. J. E. 35 (2012). doi:10.1140/epje/i2012-12041-x.

[23] A.B. Silva, C. Wisniewski, J.V.A. Esteves, R. Gregorio, Effect of Drawing on the Crystal–Amorphous Interphase, Remanent Polarization and Dielectric Properties of α-PVDF Films, Ferroelectrics. 413 (2011) 220–230. doi:10.1080/00150193.2011.554263.

[24] T. Prabhakaran, J. Hemalatha, Ferroelectric and magnetic studies on unpoled Poly (vinylidine Fluoride)/Fe_3O_4 magnetoelectric nanocomposite structures, Mater. Chem. Phys. 137 (2013) 781–787. doi:10.1016/J.MATCHEMPHYS.2012.09.064.

[25] C. Tsonos, N. Soin, G. Tomara, B. Yang, G.C. Psarras, A. Kanapitsas, E. Siores, Electromagnetic wave absorption properties of ternary poly(vinylidene fluoride)/magnetite nanocomposites with carbon nanotubes and graphene, RSC Adv. 6 (2016) 1919–1924. doi:10.1039/C5RA24956B.

[26] H. Wang, Q. Fu, J. Luo, D. Zhao, L. Luo, W. Li, Three-phase Fe_3O_4

/MWNT/PVDF nanocomposites with high dielectric constant for embedded capacitor, Appl. Phys. Lett. 110 (2017) 242902. doi:10.1063/1.4986443.

[27] C. Chanmal, J. Jog, Dielectric Relaxation Spectroscopy for Polymer Nanocomposites, in: Charact. Tech. Polym. Nanocomposites, Wiley-VCH Verlag GmbH & Co. KGaA, Weinheim, Germany, 2012: pp. 167–184. doi:10.1002/9783527654505.ch7.

[28] Z.-W. Ouyang, E.-C. Chen, T.-M. Wu, Thermal Stability and Magnetic Properties of Polyvinylidene Fluoride/Magnetite Nanocomposites, Materials (Basel). 8 (2015) 4553–4564. doi:10.3390/ma8074553.

[29] E. Assouline, A. Lustiger, A.H. Barber, C.A. Cooper, E. Klein, E. Wachtel, H.D. Wagner, Nucleation ability of multiwall carbon nanotubes in polypropylene composites, J. Polym. Sci. Part B Polym. Phys. 41 (2003) 520–527. doi:10.1002/polb.10394.

[30] M. Mičušík, M. Omastová, J. Pionteck, C. Pandis, E. Logakis, P. Pissis, Influence of surface treatment of multiwall carbon nanotubes on the properties of polypropylene/carbon nanotubes nanocomposites, Polym. Adv. Technol. 22 (2011) 38–47. doi:10.1002/pat.1745.

[31] A.R. Bhattacharyya, T. V. Sreekumar, T. Liu, S. Kumar, L.M. Ericson, R.H. Hauge, R.E. Smalley, Crystallization and orientation studies in polypropylene/single wall carbon nanotube composite, Polymer (Guildf). 44 (2003) 2373–2377. doi:10.1016/S0032-3861(03)00073-9.

[32] A.S. Bhatt, D.K. Bhat, M.S. Santosh, Crystallinity, conductivity, and magnetic properties of PVDF-Fe_3O_4 composite films, J. Appl. Polym. Sci. 119 (2011) 968–972. doi:10.1002/app.32796.

[33] C. Xu, C. Ouyang, R. Jia, Y. Li, X. Wang, Magnetic and optical properties of poly(vinylidene difluoride)/Fe_3O_4 nanocomposite prepared by coprecipitation approach, J. Appl. Polym. Sci. 111 (2009) 1763–1768. doi:10.1002/app.29194.

[34] Z.-M. Dang, Y.-H. Lin, C.-W. Nan, Novel Ferroelectric Polymer Composites with High Dielectric Constants, Adv. Mater. 15 (2003) 1625–1629. doi:10.1002/adma.200304911.

[35] R. Gonçalves, P.M. Martins, C. Caparrós, P. Martins, M. Benelmekki, G. Botelho, S. Lanceros-Mendez, A. Lasheras, J. Gutiérrez, J.M. Barandiarán, Nucleation of the electroactive β-phase, dielectric and magnetic response of poly(vinylidene fluoride) composites with Fe_2O_3 nanoparticles, J. Non. Cryst. Solids. 361 (2013) 93–99. doi:10.1016/j.jnoncrysol.2012.11.003.

[36] A. Linares, A. Nogales, D.R. Rueda, T.A. Ezquerra, Molecular dynamics in PVDF/PVA blends as revealed by dielectric loss spectroscopy, J. Polym. Sci. Part B Polym. Phys. 45 (2007) 1653–1661. doi:10.1002/polb.21210.

[37] Y. Zhang, M. Zuo, Y. Song, X. Yan, Q. Zheng, Dynamic rheology and dielectric relaxation of poly(vinylidene fluoride)/poly(methyl methacrylate) blends, Compos. Sci. Technol. 106 (2015) 39–46. doi:10.1016/J.COMPSCITECH.2014.10.024.

[38] H. Rekik, Z. Ghallabi, I. Royaud, M. Arous, G. Seytre, G. Boiteux, A. Kallel, Dielectric relaxation behaviour in semi-crystalline polyvinylidene fluoride (PVDF)/TiO_2 nanocomposites, Compos. Part B Eng. 45 (2013) 1199–1206. doi:10.1016/j.compositesb.2012.08.002.

[39] C. Thirmal, C. Nayek, P. Murugavel, V. Subramanian, Magnetic, dielectric and magnetodielectric properties of PVDF-$La_{0.7}Sr_{0.3}MnO_3$ polymer

nanocomposite film, AIP Adv. 3 (2013) 112109. doi:10.1063/1.4830282.

[40] P. Martins, C.M. Costa, G. Botelho, S. Lanceros-Mendez, J.M. Barandiaran, J. Gutierrez, Dielectric and magnetic properties of ferrite/poly(vinylidene fluoride) nanocomposites, Mater. Chem. Phys. 131 (2012) 698–705. doi:10.1016/J.MATCHEMPHYS.2011.10.037.

[41] A. Bello, E. Laredo, M. Grimau, Distribution of relaxation times from dielectric spectroscopy using Monte Carlo simulated annealing: Application to α − PVDF, Phys. Rev. B. 60 (1999) 12764–12774. doi:10.1103/PhysRevB.60.12764.

[42] A. Patsidis, G.C. Psarras, Dielectric behaviour and functionality of polymer matrix - Ceramic $BaTiO_3$ composites, Express Polym. Lett. 2 (2008) 718–726. doi:10.3144/expresspolymlett.2008.85.

[43] C.G. Raptis, A. Patsidis, G.C. Psarras, Electrical response and functionality of polymer matrix-titanium carbide composites, Express Polym. Lett. 4 (2010) 234–243. doi:10.3144/expresspolymlett.2010.30.

[44] E. Tuncer, M. Wegener, R. Gerhard-Multhaupt, Distribution of relaxation times in α-phase polyvinylidene fluoride, J. Non. Cryst. Solids. 351 (2005) 2917–2921. doi:10.1016/j.jnoncrysol.2005.03.055.

[45] Y. Liu, J.Y. Lee, L. Hong, Morphology, crystallinity, and electrochemical properties ofin situ formed poly(ethylene oxide)/TiO_2 nanocomposite polymer electrolytes, J. Appl. Polym. Sci. 89 (2003) 2815–2822. doi:10.1002/app.12487.

[46] N.G. McCrum, B.E. Read, G. Williams, Anelastic and Dielectric Effects in Polymeric Solids, John Wiley & Sons Ltd, London, 1967.

[47] G.M. Tsangaris, G.C. Psarras, N. Kouloumbi, Electric modulus and interfacial polarization in composite polymeric systems, J. Mater. Sci. 33 (1998) 2027–2037. doi:10.1023/A:1004398514901.

[48] H. Hammami, M. Arous, M. Lagache, A. Kallel, Study of the interfacial MWS relaxation by dielectric spectroscopy in unidirectional PZT fibres/epoxy resin composites, J. Alloys Compd. 430 (2007) 1–8. doi:10.1016/J.JALLCOM.2006.04.048.

[49] C. V. Chanmal, J.P. Jog, Dielectric relaxations in PVDF/$BaTiO_3$ nanocomposites, Express Polym. Lett. 2 (2008) 294–301. doi:10.3144/expresspolymlett.2008.35.

[50] M. Hernández, J. Carretero-González, R. Verdejo, T.A. Ezquerra, M.A. López-Manchado, Molecular Dynamics of Natural Rubber/Layered Silicate Nanocomposites As Studied by Dielectric Relaxation Spectroscopy, Macromolecules. 43 (2010) 643–651. doi:10.1021/ma902379t.

[51] H.W. Starkweather, P. Avakian, Conductivity and the electric modulus in polymers, J. Polym. Sci. Part B Polym. Phys. 30 (1992) 637–641. doi:10.1002/polb.1992.090300614.

[52] G.M. Tsangaris, G.C. Psarras, Dielectric response of a polymeric three-component composite, J. Mater. Sci. 34 (1999) 2151–2157. doi:10.1023/A:1004528330217.

[53] J. Mijović, H. Lee, J. Kenny, J. Mays, Dynamics in Polymer−Silicate Nanocomposites As Studied by Dielectric Relaxation Spectroscopy and Dynamic Mechanical Spectroscopy, Macromolecules. 39 (2006) 2172–2182. doi:10.1021/ma051995e.

[54] G.C. Psarras, Conductivity and dielectric characterization of polymer nanocomposites, Phys. Prop. Appl. Polym. Nanocomposites. (2010) 31–69. doi:10.1533/9780857090249.1.31.

[55] S.A. Madbouly, J.U. Otaigbe, Broadband dielectric spectroscopy of nanostructured maleated polypropylene/polycarbonate blends prepared by in situ polymerization and compatibilization, Polymer (Guildf). 48 (2007) 4097–4107. doi:10.1016/J.POLYMER.2007.05.020.

[56] H.Y. Guney, T. Oskay, H.S. Ozkan, Mechanical anisotropy in biaxially oriented polyvinyl chloride, J. Polym. Sci. Part B Polym. Phys. 29 (1991) 897–906. doi:10.1002/polb.1991.090290801.

[57] Q. Xiao, L. Li, B. Qing Zhang, X. Ming Chen, Polyvinylidene fluoride-modified $BaTiO_3$ composites with high dielectric constant and temperature stability, Ceram. Int. 39 (2013) S3–S7. doi:10.1016/J.CERAMINT.2012.10.025.

[58] J. van Turnhout, M. Wübbenhorst, Analysis of complex dielectric spectra. I. One-dimensional derivative techniques and three-dimensional modelling, J. Non. Cryst. Solids. 305 (2002) 50–58. doi:10.1016/S0022-3093(02)01086-4.

[59] ASTM D3426-97, Standard Test Method for Dielectric Breakdown Voltage and Dielectric Strength of Solid Electrical Insulating Materials Using Impulse Waves 1, Test. 97 (2015) 2–5. doi:10.1520/D3426-97R12.2.

[60] T. Tanaka, Dielectric nanocomposites with insulating properties, IEEE Trans. Dielectr. Electr. Insul. 12 (2005) 914–928. doi:10.1109/TDEI.2005.1522186.

Figures captions

Figure 1. SEM images of cryo-fractured PVDF-Fe_3O_4 samples containing (a) 5 and (b) 15 wt% Fe_3O_4.

Figure 2. (a) Comparative relative TGA curves as a function of temperature for all the nanocomposites studied and differential TGA curves as a function of temperature. (b) The temperature corresponding to 5% initial mass loss as a function of the filler concentration (left axis) and the maximum weight loss rate as a function of filler content for the nanocomposite systems studied (right axis).

Figure 3. (a) DSC thermograms showing melting during first heating, (b) crystallization during cooling.

Figure 4. Variation of (a) dielectric permittivity and (b) loss tan δ as a function of frequency, for all the examined systems, at 30^{o}C.

Figure 5. Electric modulus loss index as a function of (a) frequency at 100^{o}C and (b) temperature at 0.1 Hz, for all the examined systems.

Figure 6. Arrhenius diagram (a) for the crystalline α_c - relaxation and (b) for MWS mechanism.

Figure 7. AC breakdown event at 69 seconds for the PVDF with 10 wt % Fe_3O_4 nanoparticles.

Figure 8. Digital photographs of the samples after the AC breakdown test; (a) pristine PVDF, (b) PVDF/5 wt% Fe_3O_4, (c) PVDF/10 wt% Fe_3O_4 and (d) PVDF/15 wt% Fe_3O_4.

Figure 9. Indicative switching impulse stressing of the PVDF/10 wt% Fe_3O_4 nanocomposites films.

Table I. Results from DSC measurements.

	1st Run			2nd Run	
	T_{m1}(°C)	T_{m2}(°C)	T_c (°C)	T_{m2}(°C)	%X_c
Sample			**(Cooling)**		**(Heating)**
PVDF	167.7	174.9	137.6	174.3	46
5% Fe_3O_4	166.8	173.5	143.1	172.7	47
10% Fe_3O_4	166.3	172.8	141.1	173.5	48
15% Fe_3O_4	165.7	172.8	141.0	173.0	44

Table II. Activation energy values of α_c- mode and MWS relaxation for all examined systems.

	Activation Energy (eV)	
	α_c- mode	MWS relaxation
PVDF	0.90	1.57
PVDF+5%Fe_3O_4	0.94	0.50
PVDF+10%Fe_3O_4	0.98	0.88
PVDF+15%Fe_3O_4	0.94	0.92

Table III. Dielectric strength of the understudyied nanocomposites and their matrix with thickness 1 mm.

Nanocomposite	Breakdown Voltage (kV)
Pure PVDF	21.90
PVDF + 5 wt% Fe_3O_4	21.75
PVDF + 10 wt% Fe_3O_4	17.30
PVDF + 15 wt% Fe_3O_4	9.35

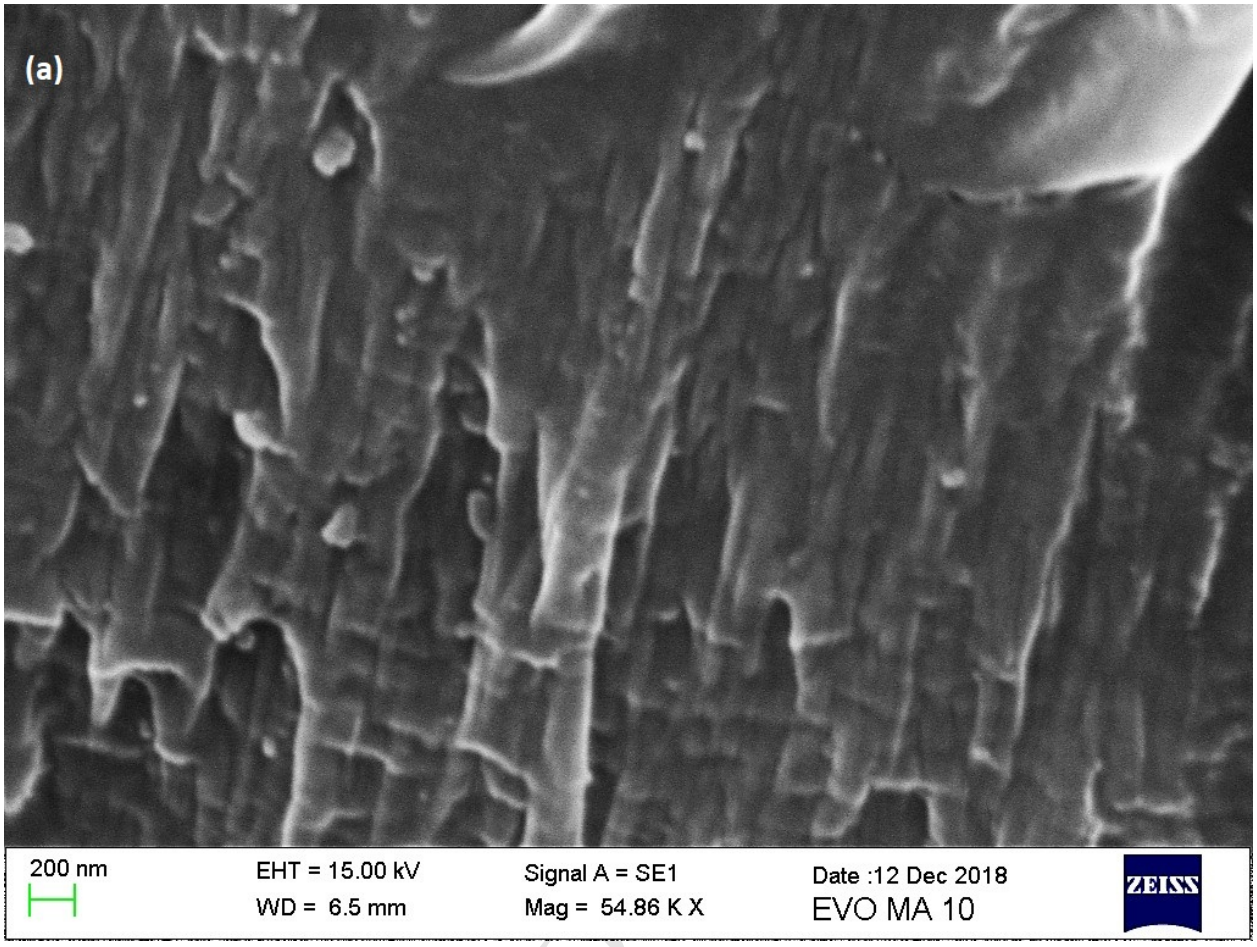
(a)
200 nm
EHT = 15.00 kV
WD = 6.5 mm
Signal A = SE1
Mag = 54.86 K X
Date :12 Dec 2018
EVO MA 10
ZEISS

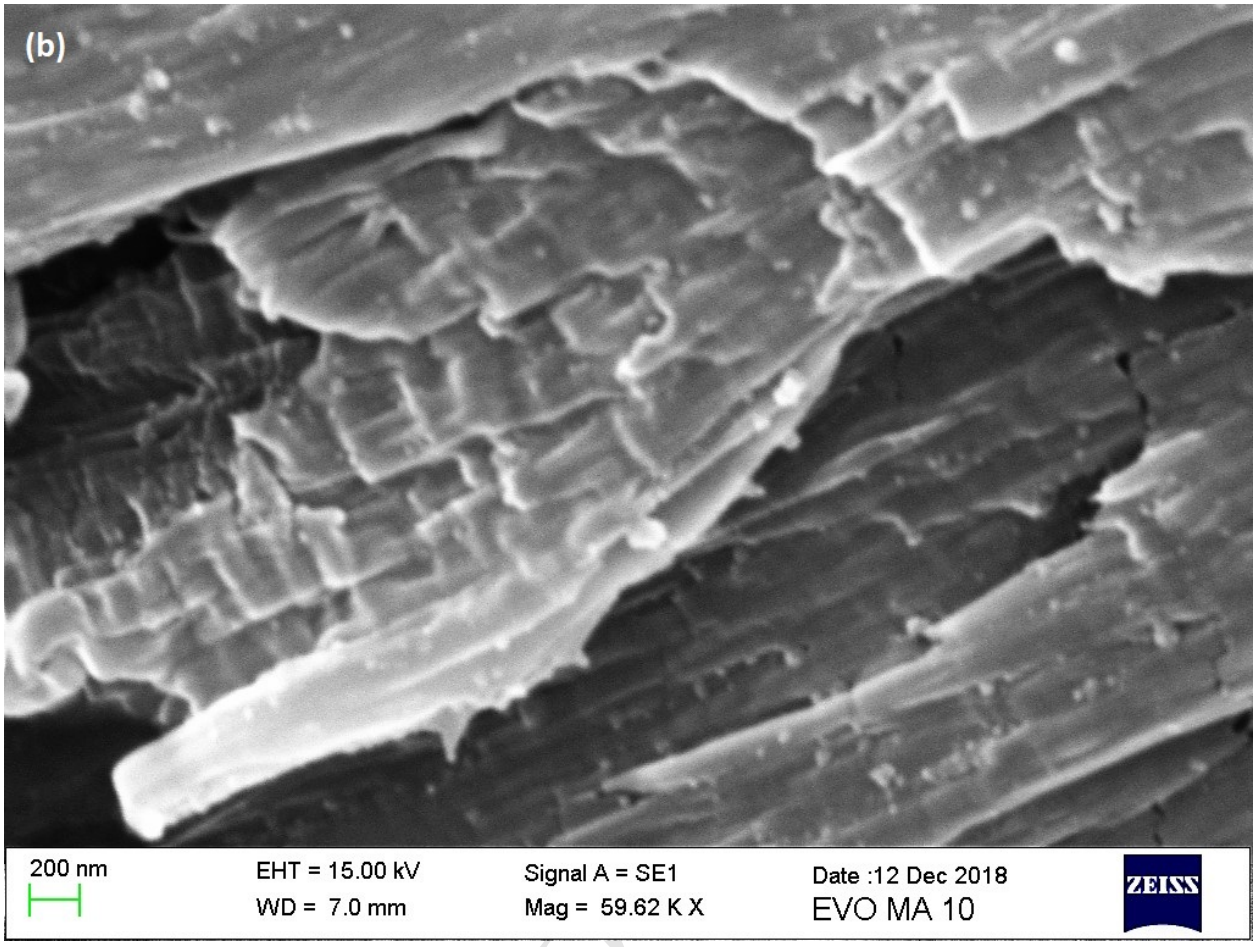
(b)
200 nm
EHT = 15.00 kV
WD = 7.0 mm
Signal A = SE1
Mag = 59.62 K X
Date :12 Dec 2018
EVO MA 10
ZEISS

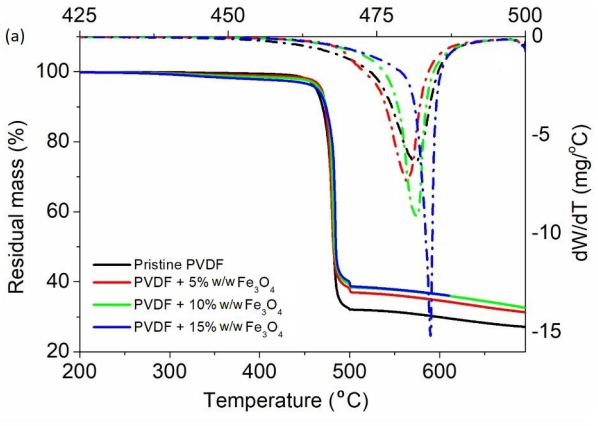

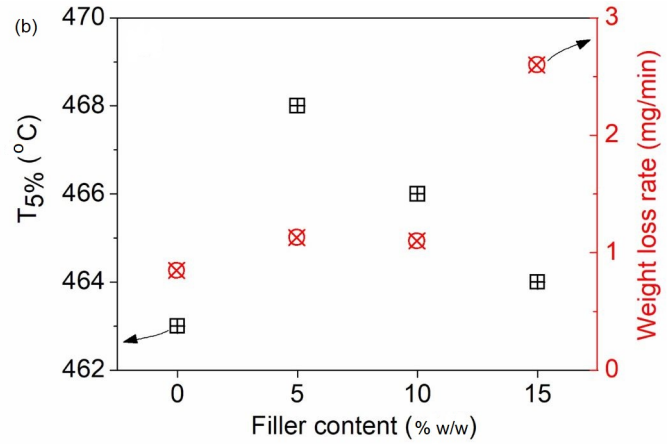

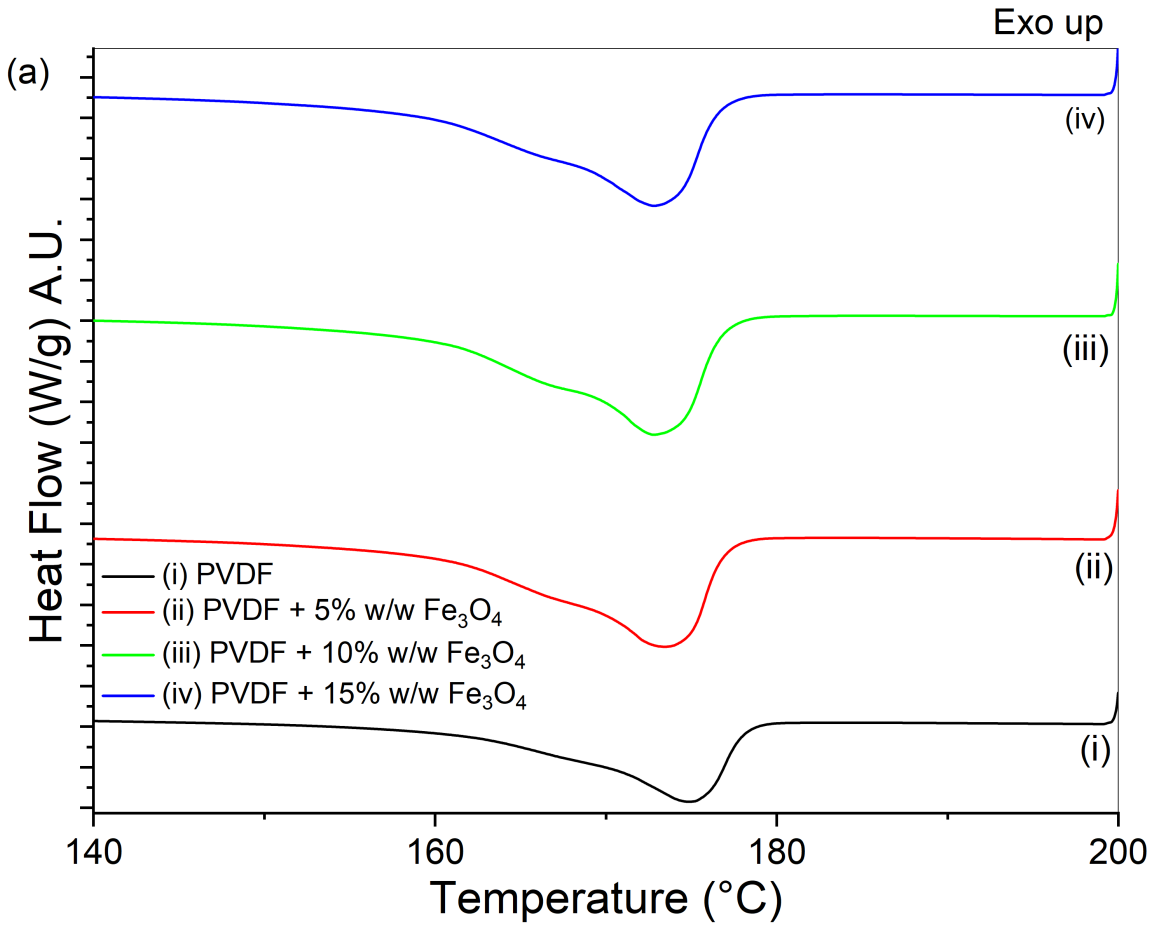
Exo up
(a)
Heat Flow (W/g) A.U.
(i) PVDF
(ii) PVDF + 5% w/w Fe3O4
(iii) PVDF + 10% w/w Fe3O4
(iv) PVDF + 15% w/w Fe3O4
(i)
(ii)
(iii)
(iv)
140
160
180
200
Temperature (°C)

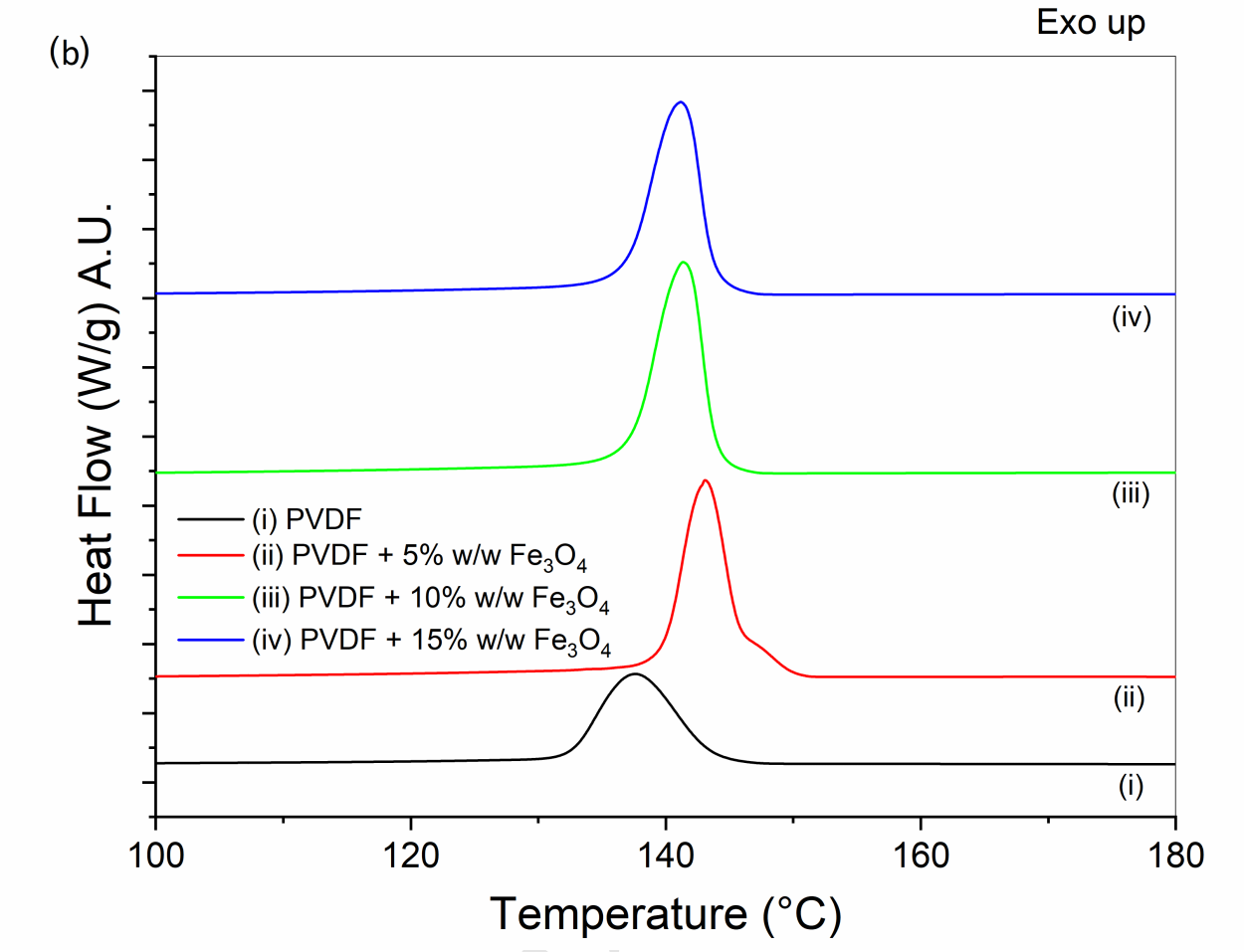
(b)
Exo up
Heat Flow (W/g) A.U.
(i) PVDF
(ii) PVDF + 5% w/w Fe3O4
(iii) PVDF + 10% w/w Fe3O4
(iv) PVDF + 15% w/w Fe3O4
(iv)
(iii)
(ii)
(i)
100
120
140
160
180
Temperature (°C)

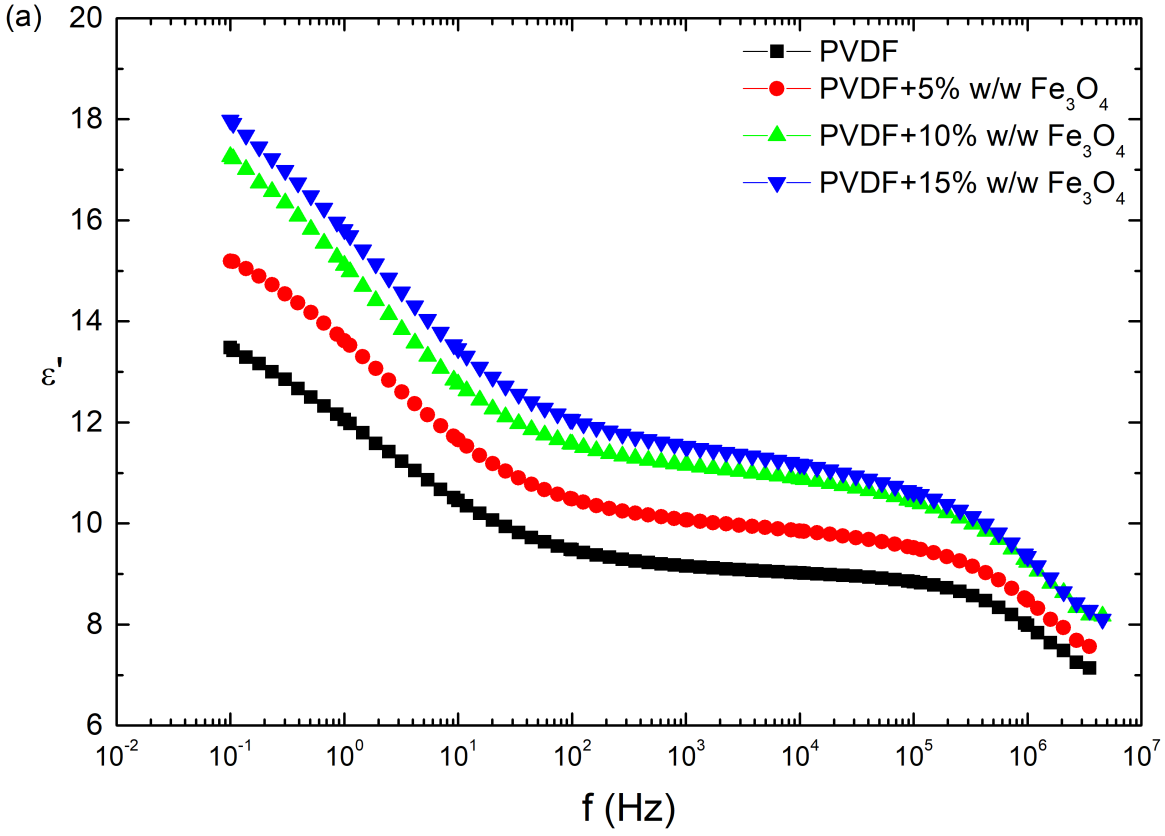

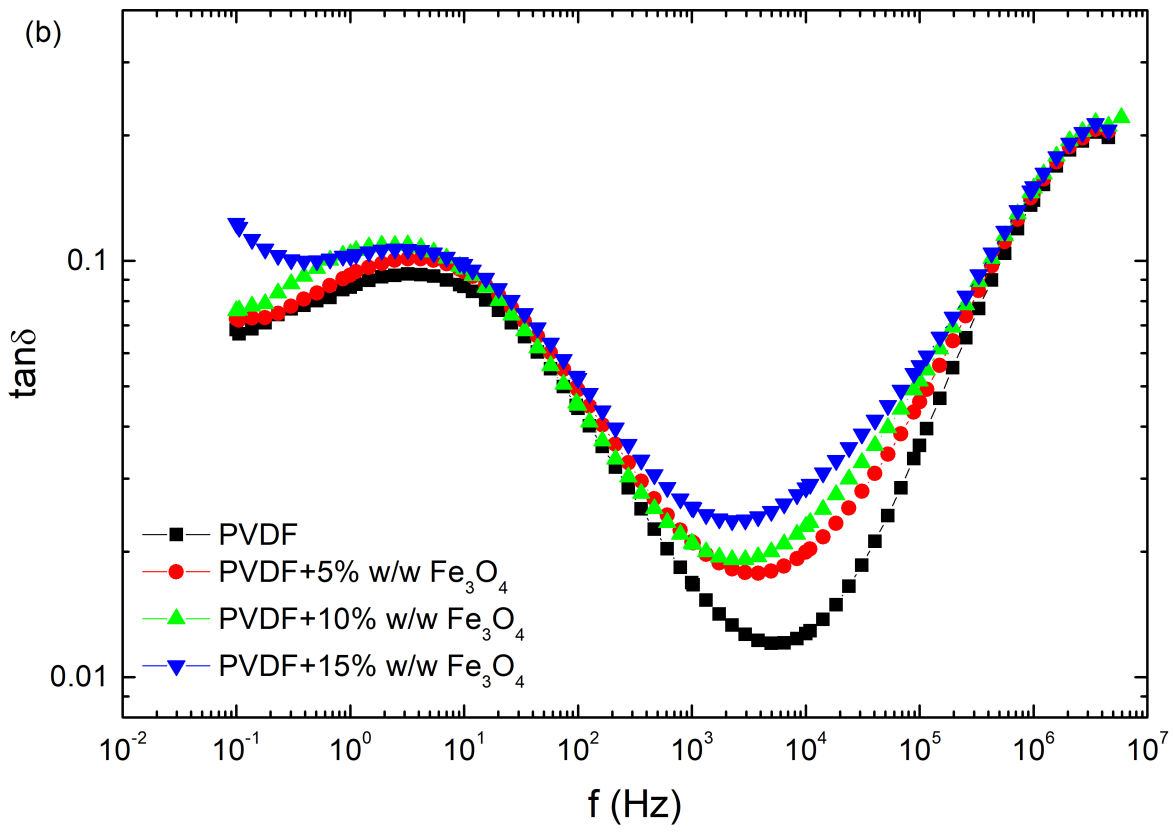

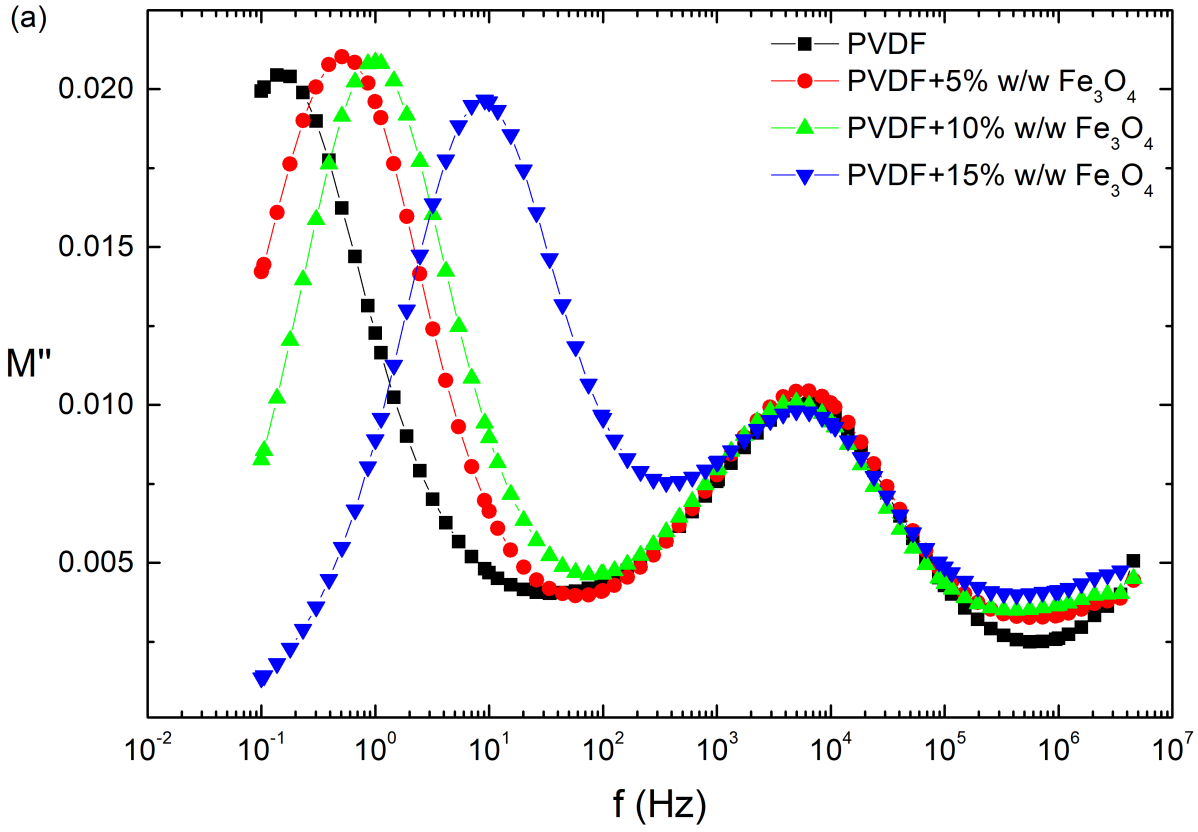

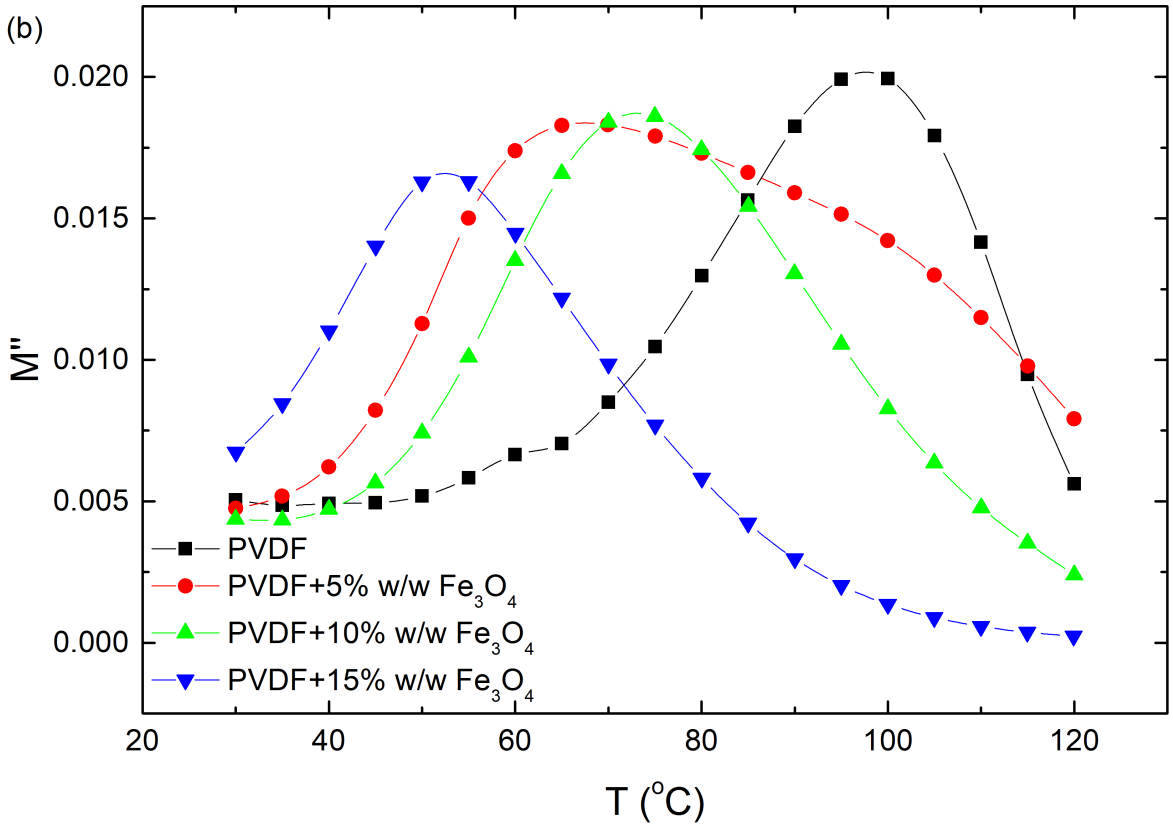

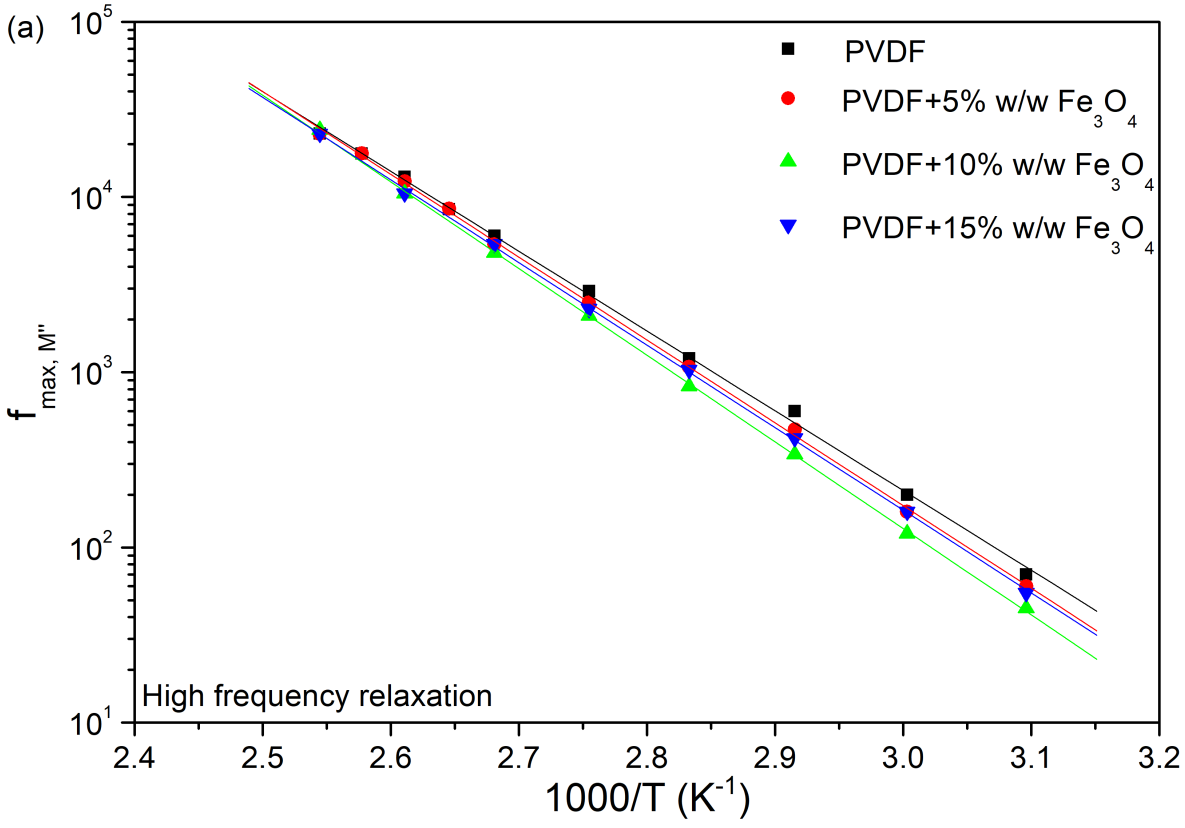

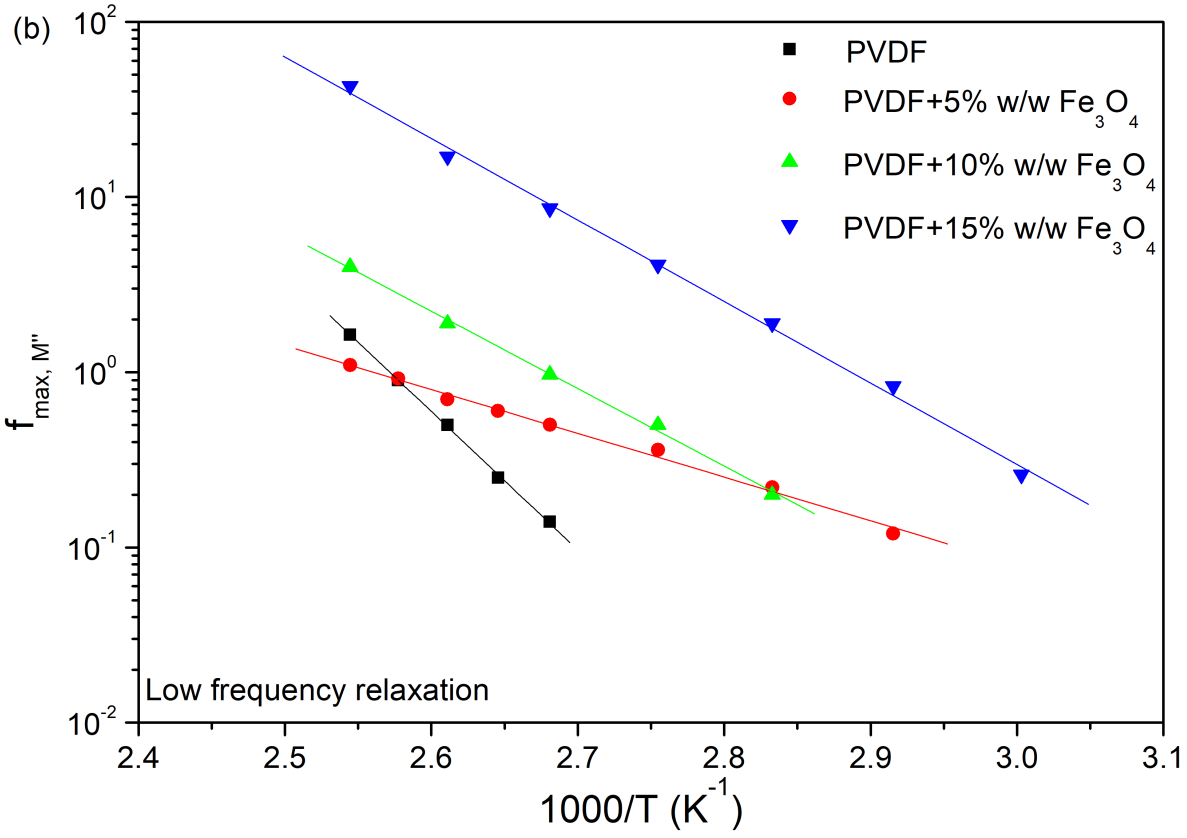

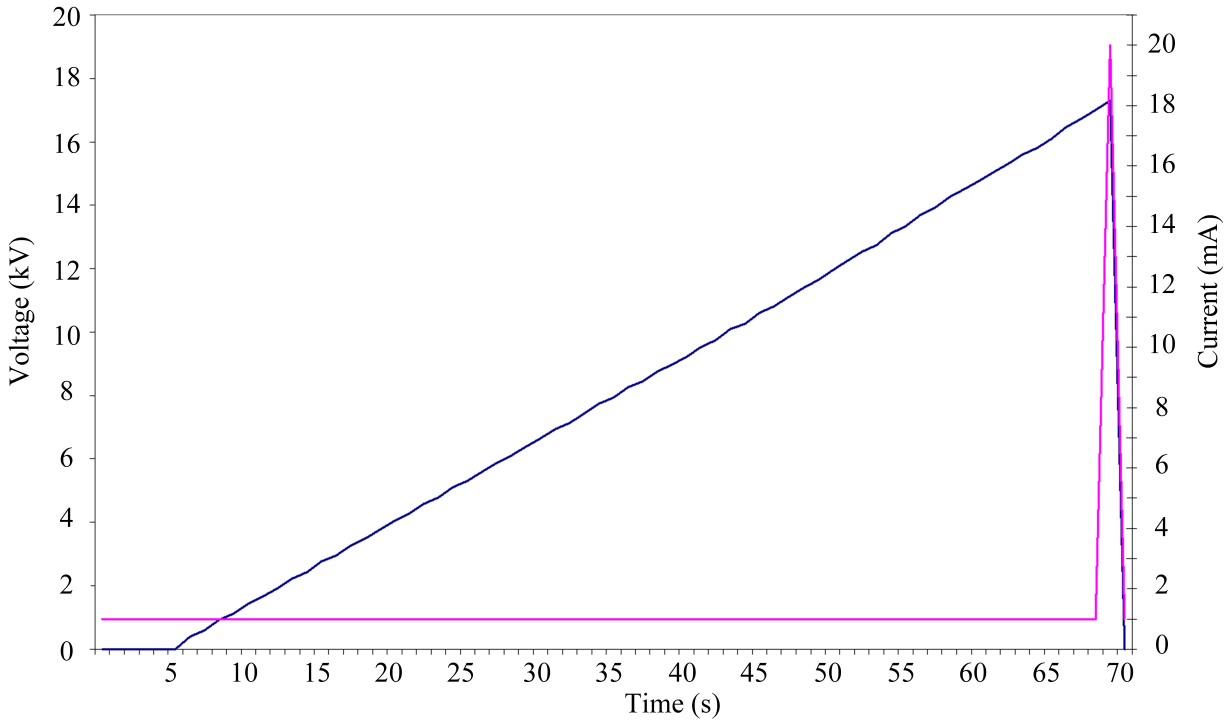

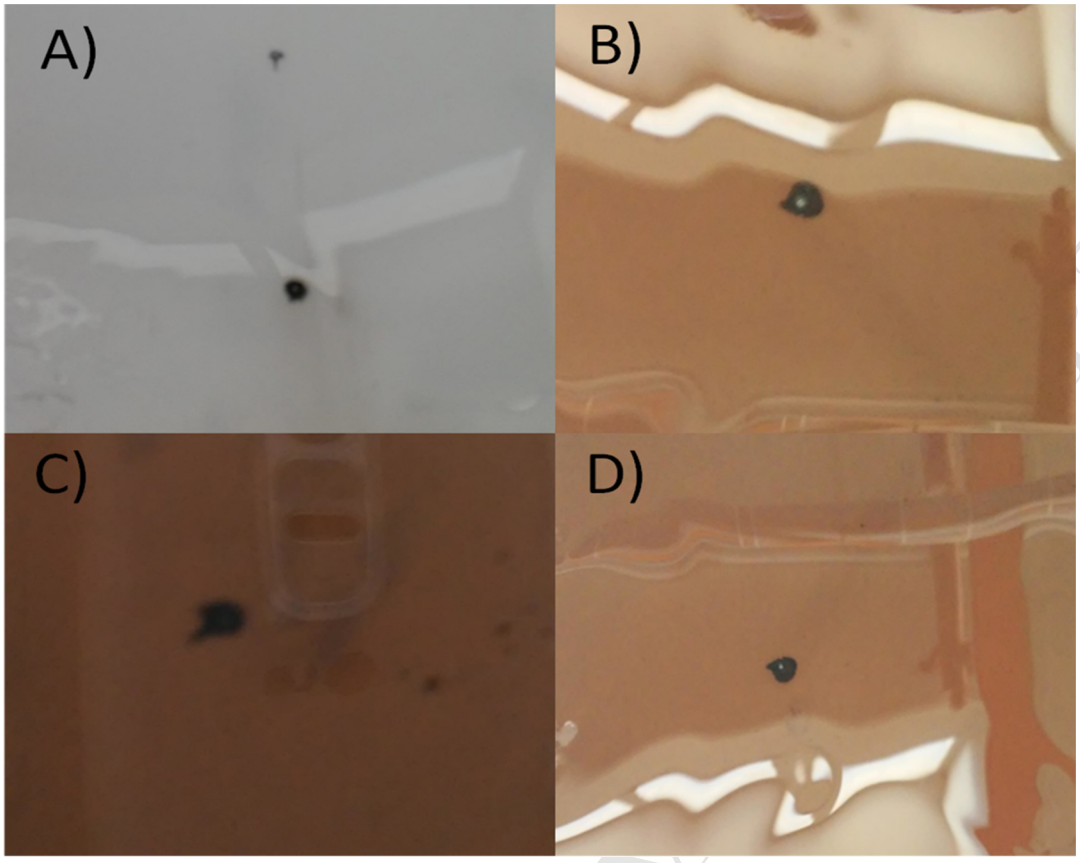

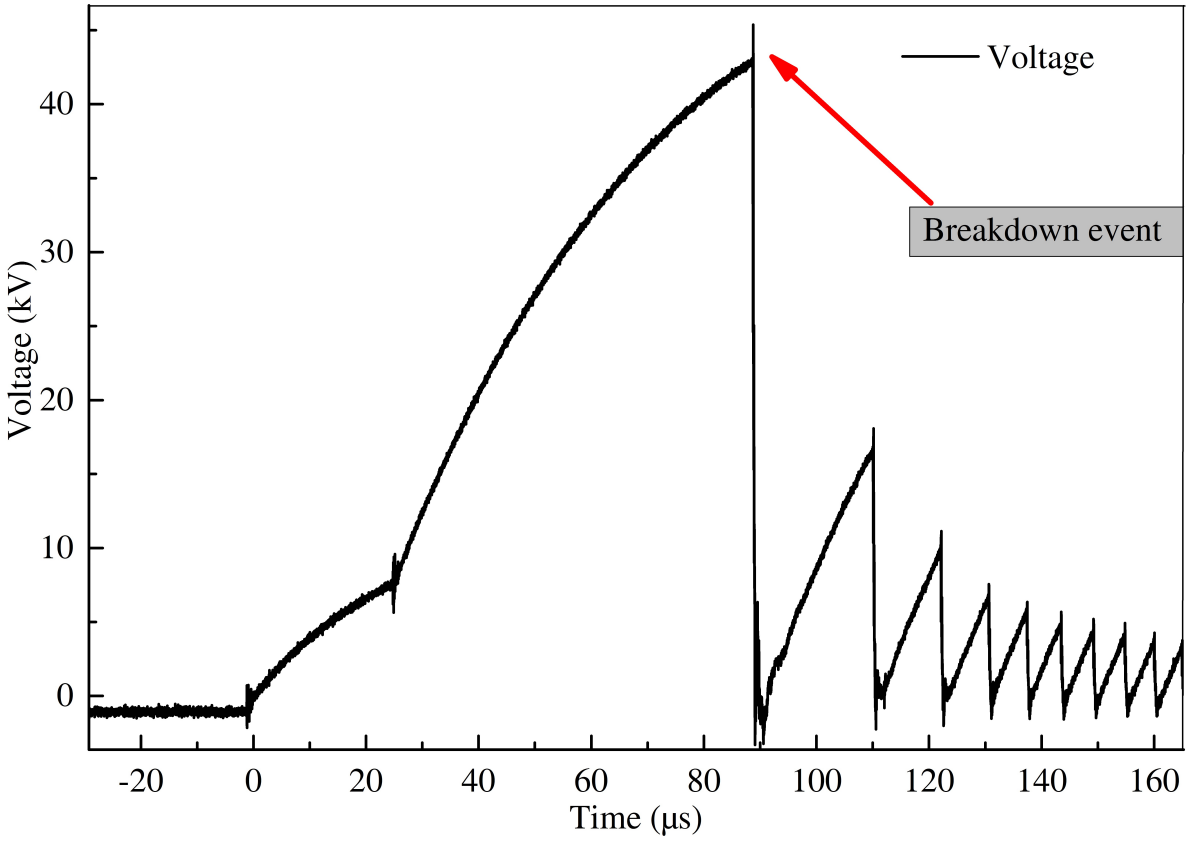

- At higher Fe_3O_4 content, the degradation temperatures became marginally higher.
- In general, the degree of crystallinity slightly increases with Fe_3O_4.
- Recorded dielectric relaxations are, α_c-relaxation and MWS interfacial polarization.
- Fe_3O_4/PVDF nanocomposites demonstrated a breakdown voltage level of 40-42kV.